# Computational Model of an Offshore Monopile Wind Turbine

Miguel Francisco Cantinho Viana
miguel.viana@tecnico.ulisboa.pt

Instituto Superior Técnico, Universidade de Lisboa, Portugal

June 2018

**Abstract**

Offshore wind energy is a renewable source with strong prospects of development, allowing both the reduction of greenhouse gas emissions and the achievement of energy independence. Nowadays, floating wind solutions are under development, since they are suited for bigger depths. However, fixed-bottom foundations are the most used by farm operators, namely the monopile foundation, due to its low production and installation costs, when compared with more costly platforms, such as jacket or tripod foundations. In this work, a monopile foundation for offshore wind power in the Portuguese coast is studied for its structural integrity. Thereby, an appropriate numerical model for the structural analysis of the foundation and tower was developed. FAST 8, an aero-hydro-servo-elastic numerical code that can compute aerodynamic and hydrodynamic loads on a running wind turbine, was used to obtain the loads applied on the structure. These loads are pre-processed before their input on a finite element model, developed using ANSYS 16 software. The grout connection, which connects the monopile to the transition piece through friction, is modeled under a changing-status nonlinearity condition. To model the soil-pile interaction, the p-y model was used, by means of the ANSYS APDL commands. Static and transient structural analyses allow the study of the structure's suitability for use in offshore environments. Different soil interactions are modeled, and their results are compared in the transient and modal analysis.

**Keywords:** Offshore wind, monopile, structural analysis, p-y model, scour depth, finite element method.

## 1. Introduction

Society is increasingly aware of pollution and the harmful effects that nonrenewable resources cause on the environment. Governments recognize that renewable energy is one of the best solutions to the problems of raw material drainage and pollutant emissions [1]. With the development of wind energy, more offshore wind farms can be found. To produce energy, it is important that the wind flow is in laminar regime so that the transformation of energy occurs free of interference. Obstructions and surface roughness have a significant influence on turbulence and on the average wind flow velocity, resulting in the wind shade effect. For higher laminar wind flows, offshore wind has better conditions to produce electricity when compared with the onshore wind [2]. The installation away from the coast has the advantage of being able to use larger rotors, due to the easiness of transportation of its constituents in high sea, resulting in a better energetic use of the process with reduced visual impact [3].

The monopile foundation is the most commonly used solution for depths up to $36\,m$ (Figure 1). Its external diameter, thickness and penetration depth in the soil depend strongly on soil conditions, water depth, environmental conditions, design standards and the turbine they support [4]. Monopiles are the most widely used solution around the globe because these systems

have the most simplified structure and, mainly, the lowest production and transportation costs.

Figure 1 – Monopile [5].

## 1.1. External Loads

For the structural analysis and the mechanical design of the foundation, it is crucial to analyze the loads that affect the structure. When impacting the structure, wind generates aerodynamic loads. In this work, the Blade Element Momentum (BEM) method was used in the calculation of the aerodynamic forces in the structure, which approximates the three-dimensional flow around the bodies to a two-dimensional flow along its sections [6]. Waves and currents are the sources of hydrodynamic loads. The method used for computing these loads was the Morison method, whose main conditions are to neglect diffraction effects, refraction effects and to consider the existence of flow separation. The weight of marine life added is directly transferred to the axial load of the monopile, however the inertial and viscous forces are also increased [7]. The sea conditions modeling did not consider turbulence or corrosion, so the propagation of cracks in a corrosive fatigue environment was not taken into account when this is considered to be one of the structures' most common operating problems in maritime environments [8]. It is important to understand that the dynamics of the rotor significantly influence the vibration of the structure. It is essential that the operating vibration frequencies of the system do not approach their natural frequencies. Since the turbine of the present work operates between $6{,}9\,rpm$ and $12{,}1\,rpm$, the 1P frequencies vary between $[0{,}115; 0{,}202]\,Hz$ and the 3P frequencies between $[0{,}345; 0{,}605]\,Hz$.

## 1.2. Structural Connections

The union between the monopile and the transition piece is guaranteed by the grout connection (Figure 2). The transition piece is placed after fixing the monopile into the soil bed, allowing to correct geometric imperfections that appear during its installation phase. Grout is a cementitious material with high mechanical resistance to compression, high internal cohesion and possesses high resistance to fatigue. The load transfer between the monopile and the transition part is carried out mainly by friction and it is the normal compression stress applied at the contact interfaces that produce the desired shear stress [9]. It is essential that there is no adhesion between the grout and the steel so that the maximum tensile stress achieved in grout is within the safety values. This is since the grout is a very brittle material towards traction $\left(\frac{\sigma_t}{\sigma_c} \cong 0{,}23\right)$ [10].

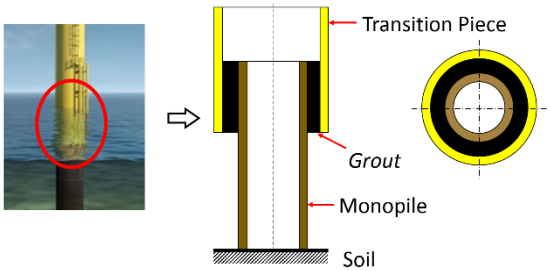


Figure 2 – Cylindrical grout connection representation for the monopile foundation.

When the introduction of the grout connection in the offshore wind turbines began, it was proved that a cylindrical connection without shear keys was able to achieve the required functionalities. However, a new solution was born, based on the design of a conical connection. By imposing some slope in the bonding zone, a resulting vertical force is ensured by the vector sum of the normal and tangential components of the steel reaction with grout [10].

Monopile design requires a detailed study of soil behavior, as it can be classified into several forms (formation process, grain size, age, mineralogic content, etc.). The stress-strain relationship for soil is nonlinear, with the strength and stiffness properties strongly

depending on stress history. The cyclic loads that soil undergoes, through pile-soil interaction, produce extensions that, due to the plasticity of the associated material, accumulate over time.

The p-y model, developed by the API (American Petroleum Institute), is nowadays the most accepted in the industry and in the scientific community [11]. The interaction is defined by the p-y curves ($p = f(y, x)$), where p is the resulting force per unit length, y the deflection in the horizontal direction and x the depth (Figure 3) [12]. The p-y curves are specific to each depth, so it is customary to model the problem as a beam supported by a series of decoupled non-linear elastoplastic springs representing the soil's reaction, as can be seen in Figure 4 [12].

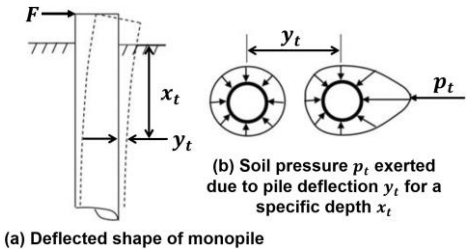


Figure 3 – p-y method of analysis for laterally loaded pile (adapted from [12]).

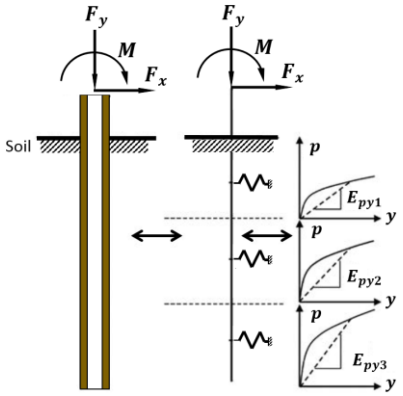


Figure 4 – p-y curves variation with depth (adapted from [12]).

Equation 1 demonstrates the expression of the p-y model for a depth $x$.

$$p = A\, p_u \tanh\left[\frac{k\, x}{A\, p_u} y\right] \quad (1)$$

In the previous equation, $p$ represents the soil's reaction, $A$ the cyclic or static load condition factor, $p_u$ the ultimate flexural strength (at a depth $x$), $k$ the initial modulus of subgrade reaction and $y$ the lateral deflection.

## 2. Methodology

### 2.1. FAST

The study of the stress states and the dynamic behavior was performed on the ANSYS software, which required aero and hydrodynamic inputs from FAST. This software is an aero-hydro-servo-elastic code that is used to simulate the response of horizontal axis wind turbines. FAST includes aerodynamic (aero), hydrodynamic (hydro), control (servo) and structural dynamic (elastic) modules, allowing a coupled simulation of the various modules. The structural dynamic module interacts with all other modules, performing the structural analysis with the information it receives from other modules [13].

### 2.2. Structural Characteristics and Case Study

The turbine used was developed by NREL, characterized by its power of 5 MW. Its structural characteristics can be found in [14]. The tower, transition piece and pile are made of steel, while grout is a cementitious material with very different properties. Unlike steel, grout is a brittle material, and, for this reason, special attention was paid to the normal positive stress that appeared in the material, during the simulations.

The chosen installation site was on the north coast of Portugal, near Póvoa de Varzim. Here, waves with a maximum significant height of $H_S = 10{,}2\ m$ and a peak period of $T_P = 11\ s$ were recorded. These values were used in the transient dynamic analyses.

Since the available data are scarce for the validation of the complex aero-hydro-servo-elastic codes, the Offshore Code Comparison Collaboration (OC3) has been created by NREL to verify the conformity of these codes. In this work, some properties of the system were considered, as defined in [15]: monopile thickness $t_{MP} = 0{,}06\ m$, base tower height ($10\ m$) and ocean depth ($20\ m$). The thickness of the transition piece considered was $0{,}06\ m$, as in the monopile. Monopile modeling in

SolidWorks was performed under these characteristics, resulting in a hollow cylinder of outer diameter $D = 6\ m$ and with the base to match the seabed surface ($z = -20\ m$). However, no additional length of the monopile's part that is in the soil (($L_{MP_S}$) was modeled in SolidWorks (Figure 5).

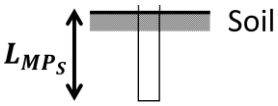


Figure 5 – Representation of the pile portion which is under the seabed $L_{MP_S}$.

## 2.3. ANSYS

### 2.3.1. Pile-Soil Interaction

$L_{MP_S}$ was modeled on ANSYS as a joint of line elements (PIPE288), so that non-linear spring elements (COMBIN39) exerted the soil reaction forces at a defined depth on a pile section (corresponding to a node of the line element). COMBIN39 has the option of being able to make a parallel discharge to the slope at the origin (representative of the elastic zone) and, thus, considering hysteresis effects [16]. This element was defined by a generalized force-deflection curve, having two nodes, one of which was fixed and the other coinciding with a node of $L_{MP_S}$. Since the deflections have a two-dimensional nature (in the plane $XY$) in each depth, two equal, perpendicular, spring elements have been defined. Each pair of perpendicular springs distanced $1\ m$ between them, vertically. The connection between the first element line (element closer to the surface of the seabed) and the solid elements was done by a fixed joint (Figure 6), responsible for the transfer of all forces and moments. The rest of the bodies were constituted by the element SOLID187. This is a tetrahedral three-dimensional element, composed of 10 nodes (with three translational degrees of freedom each), suitable for modeling irregular geometries [16].

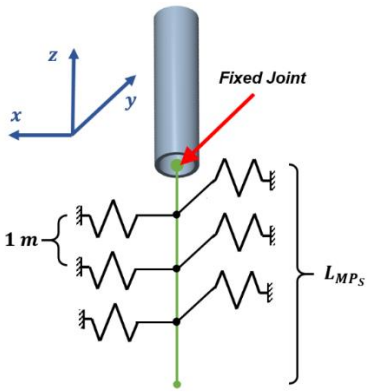


Figure 6 – Fixed Joint representation, responsible of connecting the solid elements to $L_{MP_S}$.

### 2.3.2. Grout Connection

For the grout connection, a friction type contact was defined between the surfaces which, in its physical nature, have the following characteristics [17]: surfaces do not interpenetrate; normal compressive forces and tangential frictional forces are transmitted; there are no associated tensile forces, i.e., surfaces are free to separate.

The nonlinearity of the contact, in finite elements, arise from the variation of the normal force on the surfaces, depending on the condition of the contact. For solid bodies, the most used formulations are based on corrective methods (the normal force varies according to the penetration value) (equation 2) [17].

$$F_{normal} = k_{normal} \cdot x_{penetration} + \lambda \qquad (2)$$

Equation 2 characterizes the Augmented Lagrange formulation, which is appropriate for friction problems of large deformations and, therefore, was the formulation used in this work. The contact stiffness was then calculated iteratively to minimize difficulties of convergence in the simulation.

## 2.4. Numerical Analyses

### 2.4.1. Model Simplifications

Due to the numerical complexity of the simulations involving contact, and the consequent increase of computational time, certain changes were applied in the

initial model. The grout connection was analyzed using the submodeling technique. For this reason, the introduction of a transition piece in the initial model was unnecessary since its function is directly related to the grout connection. Therefore, the tower was connected directly to the monopile. To avoid eventual errors of convergence in this connection, and since the material of the two bodies is the same, it was assumed that the tower-pile assembly was one body only. However, the thickness of the base of the tower and of the top of the pile were not equal, which could cause errors in the creation of the mesh and stress concentration. Therefore, the internal radius of the monopile was extended until it intersects the inner surface of the tower (Figure 7).

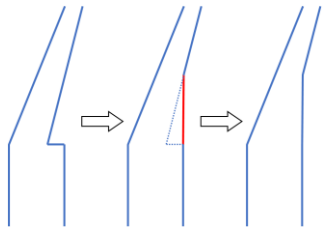

Figure 7 – Model simplification representation, not accounting the grout connection.

2.4.2. Analyses Definition

The tests that have been performed can be divided into: static structural analyses; modal analyses; transient structural analyses.

**Static Structural Analyses**

The grout connection has evolving for a conical connection. According to DNV-OS-J101 [18], the conical angle of the connection must be less than 4º. The first static analysis was performed to understand which angle best suited the problem and for that the values used were $\alpha = \{1{,}25º; 2{,}50º; 3{,}75º\}$. The thickness of the grout and the coefficient of friction between the defined materials were $t_g = 125\,mm$ and $\mu = 0{,}7$, respectively, according to DNV-ST-0126 [19]. These tests were made to study which angles supported, both axially and flexed, the turbine-tower assembly and whose configuration showed lower stress states. The transient analysis of the grout connection was done with the configuration that obtained the best results. For this static test, the complete model was used with values of force and moment applied to the top of the tower of $F = 900\,KN$ and $M = 3{,}4 \cdot 10^3\,KN \cdot m$, respectively. These values came from the maximum values of the respective variables, in a FAST simulation, for the rated wind speed, since this is the wind speed that causes the greater rotor loads.

The remaining static analysis was related to the monopile dimensioning. In order to be able to proceed with the transient analyses, an estimate of $L_{MP_S}$ was computed on this static analysis. The soil is responsible for counteracting the external loads and ensuring the equilibrium of the structure. The asymptotes of the p-y curves represent the soil's resistive capacity limit and it will be by this restriction that a pile's depth $x$ of soil penetration will not be enough to withstand the external loads. For this analysis, the values of the first static analysis were also used. The determination of the final length was achieved with an iterative process, considering that the static equilibrium had to be reached and that the maximum stress at the pile had not exceeded the safety limit defined by DNVGL-ST-0437 [20].

**Modal Analyses**

The performed modal analyses that were performed were directly related to the transient analyses. These differed according to the pile-soil interaction as follows: 1 – Clamped pile, $Enc_0$ (with no pile-soil interaction model); 2 - Penetrating pile in clays, $Arg_0$ (Portuguese case); 3 – Penetrating pile in stratified soil, $Est_0$ (OC3 case); 4 – Clamped pile and penetrating pile in clays with contribution of soil erosion, $Enc_i$ and $Arg_i$. The index $i$ corresponds to the scour depth.

The p-y curves of the different cases differed in the three main parameters that define each curve: effective soil unit weight ($\gamma$), internal friction angle ($\phi$) and initial modulus of subgrade reaction ($k$). Figure 8 demonstrates how these parameters vary. It is verified that the model 3

presents a stiffer and a more resistant soil, comparing with model 2.

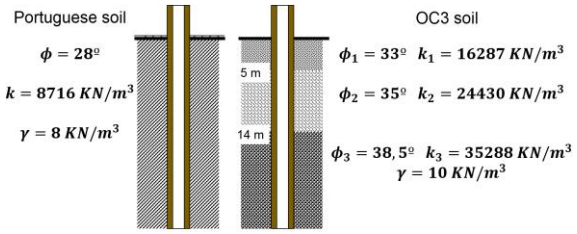


Figure 8 – Variables $\phi$, $k$ e $\gamma$ of the different soil types.

DNVGL-ST-0126 [19] states that the ratio of scour depth to pile diameter, $\frac{S}{D}$, can reach a maximum value of 1,3 for a laminar sea current [19], which means that for a pile of $D = 6\,m$, one can obtain $S = 7{,}8\,m$. The dynamic behavior of the systems (clamped and penetrating pile in clays) was analyzed for four different depths $S = \{0; 3; 5; 7\}\,m$ in order to understand how its natural frequencies were influenced. The erosion phenomenon resulted in changes in pile-soil interaction, for the $Arg_i$ models. The contact area between the pile and the soil decreased and the characteristic springs of each depth moved downwards (Figure 9). In contrast, an increase in the scour depth for the clamped pile did not change the pile-soil interaction, since soil stiffness remained infinite.

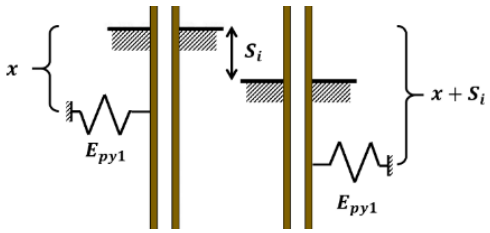


Figure 9 – Non-linear springs' translation with scour depth.

Since, for the transient analysis, the simplified model (without grout connection) was used, a comparison between the results of the modal analyzes between these models (with and without grout connection) was performed. This comparison aimed to understand if the simplification of the model was preponderant in the dynamic response of the system.

**Transient Structural Analyses**

This dissertation was centered on DLC 1.1 since the GL guidelines indicate it to find critic regions and to study its fatigue life [21]. It was used the rated wind speed ($\bar{u} = 11{,}4\,m/s$) because it is the one that causes higher rotor loads. Due to the scarcity of information of the marine life deposition for the considered location, it was used the values indicated by DNVGL-ST-0437 for normal climatic conditions (depth $= [-2; 40]\,m$; thickness $= 100\,mm$; density $= 1325\ kg \cdot m^{-3}$) [20].

The transient analyses that were carried out attempted to understand how the system responded to the external loads and to make the comparison with the different modulations of the pile-soil interaction: $Enc_0$, $Arg_0$, $Est_0$, $Enc_7$ and $Arg_7$. The sea depth for the models $Enc_7$ and $Arg_7$ was defined as $27\,m$, influencing the hydrodynamic loads in the structure, since the area of incidence of the current and the profile of its velocity is different than the other cases. In addition to the mentioned transient analyses, an extra transient analysis of the grout connection submodel was performed to study the grout connection. Displacements were assigned only in the transition piece and in the monopile, as analysis inputs, so that the grout moved only over the friction action between the bodies.

## 3. Results and Discussion

### 3.1. Static Structural Analyses

For the static analysis of the grout connection, it was found that a slight variation in $\alpha$ resulted in a significant increase of the maximum normal stress in the material. This variation is related to the decrease of the effective grout length. The tensile yield stress characteristic of the material $\sigma_t = 25{,}0\ MPa$ justifies the choice of the angle of 1,25º for the structural link, being this the configuration used in the transient analysis (Figure 10).

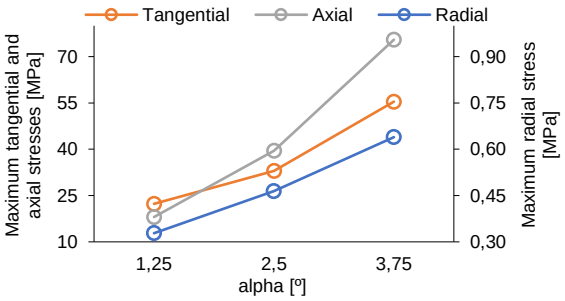


Figure 10 – Maximum normal grout stresses in axial, tangential and radial directions, with $\alpha$.

For the monopile dimensioning, the iterative process demonstrated that the equilibrium was reached easily, even for low pile penetration depths. The maximum pile stress, for these cases, was also within the safety values, however the deflections in the structure were very large. For these reasons, a length of $L_{MP_S} = 36\ m$ was defined. This configuration permitted to compare results with the OC3 model. The following two graphs correspond to the distributed reaction of the soil for models $Arg_0$ and $Est_0$. It is observable that these soils present different stiffness. The zero-deflection point is at a lower depth value, in the Portuguese case, which is an indication of a lower stiffness. In the limit case, that is, if the soil had infinite stiffness, this point would be at the seabed surface and the pile would be clamped.

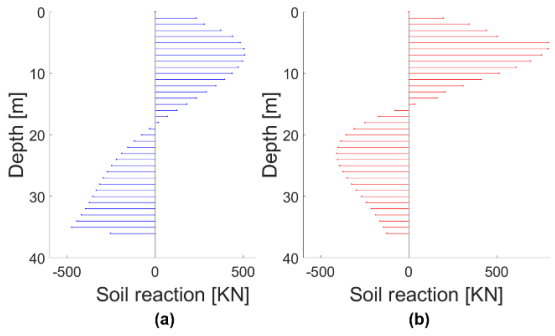


Figure 11 – Soil reaction in the (a) Portuguese and (b) OC3 cases.

## 3.2. Modal Analyses

The natural frequencies increased with soil stiffness. For a scour depth of $S = 0\ m$, the model $Enc_0$, characterized by having an infinite soil stiffness, holds the highest value frequencies, followed by the model $Est_0$ and, finally, the $Arg_0$. The first natural frequencies of the models $Enc_0$, $Est_0$ and $Arg_0$ $\left(f_{0_{Enc_0}} = 0{,}2697\ Hz, f_{0_{Est_0}} = 0{,}2411\ Hz, f_{0_{Arg_0}} = 0{,}2354\ Hz\right)$, in the side-side direction, lied between the 1P and 3P frequency bands. Ergo, the structure of these models, is of the soft-stiff type, which increases its fatigue life. On the other hand, the values of the models $Est_0$ and $Arg_0$ lied in the waves frequency band $f_{waves} = [0{,}05\ Hz; 0{,}25\ Hz]$ for the specified installation site, which is undesirable.

As discussed in 2.4.2 section, it is important to study how erosion affects the dynamic response of these systems. Figure 12 shows the decrease of the first frequencies of the systems, with the increase of scour depth, for the different pile-soil interactions ($Enc_i$ and $Arg_i$) in the side-side direction.

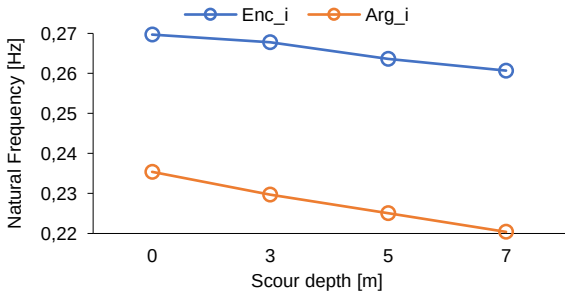


Figure 12 – Natural frequency variation with scour depth for clamped pile and pile embebed in clay.

The percentage differences recorded, between the models $Enc_0$ and $Enc_i$ and between the models $Arg_0$ and $Arg_i$, show that, considering the model p-y, an increase in the scour depth results in a more pronounced decrease of the natural frequencies of the system, when compared to a clamped pile model. This is since the soil stiffness variation itself is different. The soil stiffness in the models $Enc_i$ remained constant (infinite stiffness), while the soil stiffness of the models $Arg_i$ decreased due to the reduction of the contact area between the pile and the surrounding soil and due to the characteristic non-linear springs' deviation. Figure 12 proves the importance of scour protection since the value of the first natural frequency of the model $Arg_7$ $\left(f_{0_{Arg_7}} = 0{,}2204\ Hz\right)$ lies outside the safety zone of the 1P band. The differences

of the natural frequency values between the grout and non-grout models, with a maximum of 3.3%, show that the simplification performed did not have much influence on the system's dynamic response.

### 3.3. Transient Structural Analyses

Figure 13 shows the graph of the maximum von Mises stress value of the entire structure for the models $Arg_0$ and $Est_0$. The model $Enc_0$ presented values of maximum von Mises stresses similar to the ones found in the model $Est_0$. Since the models $Est_0$ and $Arg_0$ had the same inertia, it was possible to conclude that it was the modeling of the pile-soil interaction that played a greater role in the maximum von Mises stress difference. The maximum stresses were recorded, mainly, in the tower. This zone defines the separation between the simplified part and the non-simplified part (Figure 14).

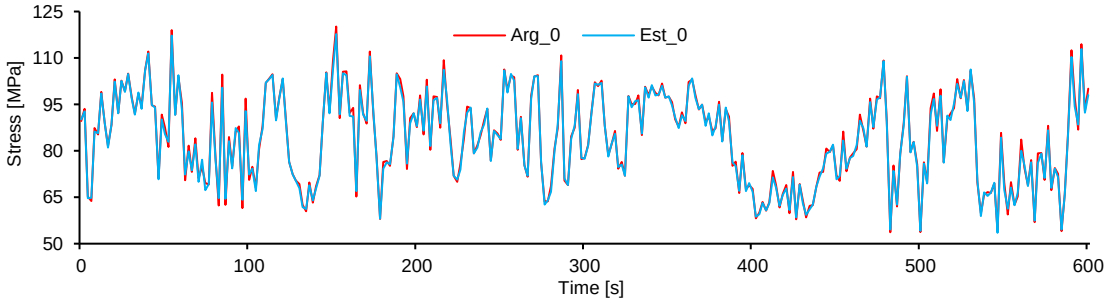


Figure 13 – Maximum von Mises stress values, in time, for $Arg_0$ and $Est_0$ models.

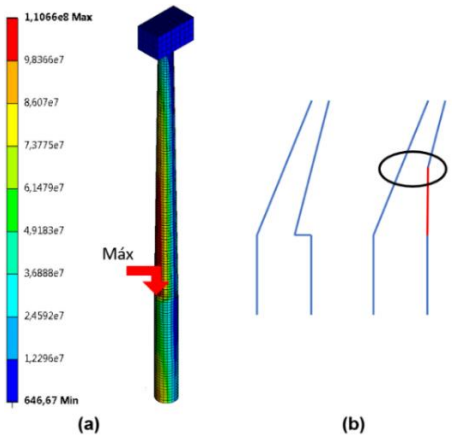


Figure 14 – (a) Global distribution of von Mises stress for $Enc_0$ model and maximum stress location; (b) Maximum von Mises stress representation.

$L_{MPS}$ stresses were evaluated separately since it was modeled by line elements. ANSYS Workbench allows evaluating axial stress values from the line elements. However, shear stress values are not counted, implying that the maximum equivalent stress is lower than expected. The shear stresses should then be accounted for a future work in order to reduce errors. The minimum axial stresses (maximum stresses, in absolute value) were recorded at the zero deflection points or, in other words, at the maximum bending moment points. Figure 15 shows the absolute value of the minimum axial stress in the line elements for the models $Arg_0$ and $Arg_7$.

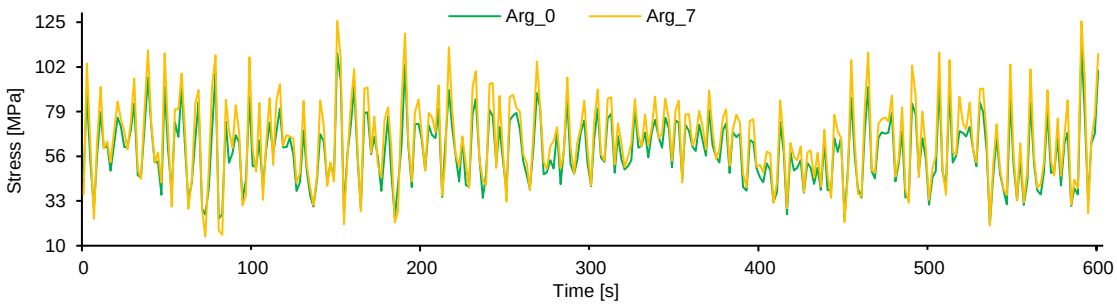


Figure 15 – Maximum absolute value of axial stress, in time, for $Arg_0$ and $Arg_7$ models.

After analyzing the results, it was intended to find an explanation of the reason that caused the model $Arg_7$ to have the highest $L_{MPS}$ stresses. Firstly, this one admitted superior loads at the seabed surface level. The bending moments were higher because all the moment arms of the outer forces increased in 7 $m$, just like the hydrodynamic forces, due to the bigger sea depth. The inertial forces were also influenced by its lower structural stiffness and, since the weight of the structure was distributed for the $L_{MPS}$ nodes, the axial reaction force was also superior to the other cases, considering its lower total number of nodes.

The maximum displacements increased with the decrease of the structural stiffness. The study of the natural frequencies and the transient analyses allowed the organization of these different models' frequencies and their maximum displacements for the generality of the simulation, respectively.

- $f_{0_{Arg_7}} < f_{0_{Arg_0}} < f_{0_{Est_0}} < f_{0_{Enc_7}} < f_{0_{Enc_0}}$;
- $d_{máx_{Enc_0}} < d_{máx_{Enc_7}} < d_{máx_{Est_0}} < d_{máx_{Arg_0}} < d_{máx_{Arg_7}}$.

Finally, the GL standard ([21]) indicates that the yield safety coefficient value should never be less than 1,1 throughout the entire finite element analysis. The structural steel stress must be $\sigma_{VM_{máx}} \leq 355/1{,}1 = 322{,}7\ MPa$ throughout the entire finite element analysis. The structural steel stress must be $\sigma_{VM} = 131{,}5\ MPa$, for the model $Enc_7$, meaning that the lowest safety coefficient obtained was 2,70.

The results obtained from the transient simulation of the grout connection submodel showed maximum values of $\sigma_{ax} = 22{,}47\ MPa$, $\sigma_{tan} = 7{,}55\ MPa$ and $\sigma_{rad} = 0{,}62\ MPa$. It was found that any of these values were found below the safety value defined by $\sigma_{t_{máx}} \leq 25/1{,}1 = 22{,}72$, when analyzed individually. The representation of the overall stress distribution in the axial direction and its critical zone can be seen in Figure 16. The maximum values were presented individually, i.e. for each direction, which may indicate that a combination of these could result in a superior normal stress exceeding safety values or, in extreme case, in reaching the yield stress. Since it is being studied a structure that is subject to cyclic loading over time, the chosen geometric configurations may not verify the fatigue resistance.

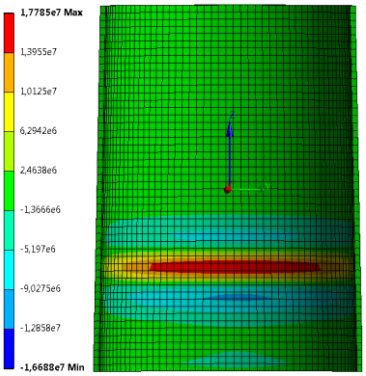


Figure 16 – Global distribution of normal axial stresses in grout, according to a section view cut in the $YZ$ plane.

## 4. Conclusions

It was verified that, in the study of dimensioning $L_{MPS}$, the static equilibrium of the structure was reached easily and that the value of the maximum equivalent stress was within the safety levels, therefore it was admitted an equal length of pile in the soil to the OC3 codes, in order to perform a comparison of results. The

modal analyzes demonstrated an increase in the value of the natural frequencies of the system for more rigid soils, as expected. It was also verified that the natural frequencies decreased with the scour depth and that these values approached the non-safe zone defined by the guidelines, justifying the scour protection that takes place in these foundations. For the transient analyzes, it was verified that the deformations in the structure were superior for the models with less stiffness and that all the models presented, predominantly, maximum stresses in the tower of the turbine. Nevertheless, these stress values were within the safety values for all the simulations. The maximum values of the normal stresses in the axial, tangential and radial directions of the grout were found in the safety interludes when analyzed individually. However, the proximity of these to the yield stress implies that the project may not verify the fatigue resistance.

## 5. References


[1] R. Miguel and D. Alves, "Acções Dinâmicas em Estruturas Offshore : Torres Eólicas em Plataformas Flutuantes," Faculdade de Ciências e Tecnologia da Universidade Nova de Lisboa, 2011.

[2] J. M. Jonkman, "Dynamics modeling and loads analysis of an offshore floating wind turbine," 2007.

[3] A. Morais Lopes, "Produção Eólica e Enquadramento Técnico-Económico em Portugal," Faculdade de Engenharia da Universidade do Porto, 2009.

[4] M. J. Kaiser and B. F. Snyder, "Offshore Wind Energy System Components," in *Offshore Wind Energy Cost Modeling*, London, United Kingdom, 2012.

[5] "Monopile weights for turbines of tomorrow." [Online]. Available: http://c2wind.com/c/cases/monopile-weights-for-turbines-of-tomorrow. [Accessed: 29-Apr-2018].

[6] P. J. Moriarty and a C. Hansen, "AeroDyn Theory Manual," 2005.

[7] J. Jonkman, A. Robertson, and G. Hayman, "HydroDyn user's guide and theory manual," *Natl. Renew. Energy Lab.*, 2015.

[8] C. Guedes Soares and R. A. Shenoi, *Analysis and Design of Marine Structures*. 2015.

[9] P. Dallyn, A. El-Hamalawi, A. Palmeri, and R. Knight, "Experimental testing of grouted connections for offshore substructures: A critical review," *Structures*, vol. 3, pp. 90–108, 2015.

[10] Y. S. Lee, B. L. Choi, J. H. Lee, S. Y. Kim, and S. Han, "Reliability-based design optimization of monopile transition piece for offshore wind turbine system," *Renew. Energy*, vol. 71, pp. 729–741, 2014.

[11] M. Bayat, L. V. Andersen, and L. B. Ibsen, "P-Y-Ẏ Curves for Dynamic Analysis of Offshore Wind Turbine Monopile Foundations," *Soil Dyn. Earthq. Eng.*, vol. 90, pp. 38–51, 2016.

[12] M. Arshad and B. C. O'Kelly, "Analysis and Design of Monopile Foundations for Offshore Wind-Turbine Structures," *Mar. Georesources Geotechnol.*, vol. 34, no. 6, pp. 503–525, 2016.

[13] B. J. Jonkman and J. M. Jonkman, "FAST v8.16.00a-bjj," 2016.

[14] J. Jonkman, S. Butterfield, W. Musial, and G. Scott, "Definition of a 5-MW Reference Wind Turbine for Offshore System Development," 2009.

[15] J. Jonkman and W. Musial, "Offshore code comparison collaboration (OC3) for IEA task 23 offshore wind technology and deployment," 2010.

[16] "Ansys Worbench Software Help Section."

[17] "Introduction to Contact - ANSYS Mechanical Structural Nonlinearities." 2010.

[18] DNV, "DNV-OS-J101 Design of Offshore Wind Turbine Structures," 2014.

[19] DNV.GL, "DNVGL-ST-0126 : Support structures for wind turbines," 2016.

[20] DNV GL, "DNVGL-ST-0437 Loads and site conditions for wind turbines," 2016.

[21] GL, "Guideline for the Certification of Offshore Wind Turbine," 2012.